

## Article

# Study on the Protection Effect of Sprinklers on Glass by Fire Scale in Building Fires

Jia Gui <sup>1</sup>, Dong Wang <sup>1</sup>, Yaqiang Jiang <sup>2,\*</sup>, Junjun Liu <sup>2</sup> and Lizhong Yang <sup>1,\*</sup>

<sup>1</sup> State Key Laboratory of Fire Science, University of Science and Technology of China, Hefei 230026, China; guijia@mail.ustc.edu.cn (J.G.); bosswang@mail.ustc.edu.cn (D.W.)

<sup>2</sup> Sichuan Fire Research Institute of MEM, Chengdu 610036, China; liujunjun@scfri.cn

\* Correspondence: jiang.yaqiang@scfri.cn (Y.J.); yanglz@ustc.edu.cn (L.Y.)

**Abstract:** Window sprinklers are commonly used to protect glass, but there is a lack of research on the effect of fire scale on protection. In this study, full-scale experiments on sprinkler-protected glass in building fires were carried out. The experimental process was simulated using CFD numerical simulation software (FDS), and the effect of the heat release rate on the protection effect was revealed based on the glass surface temperature and heat insulation efficiency. It was found that in a full-size compartment fire, the window sprinkler was able to protect the glass from being damaged by high-temperature smoke. The numerical simulation could effectively simulate the spray distribution pattern of a window sprinkler as well as the gas temperature evolution, and the simulation results matched well with the full-size experiments. The window surface temperatures all decreased rapidly and increased linearly with the HRR after the window sprinkler was activated. The steady-state window center temperatures were 40 °C, 60 °C and 76 °C when the HRR was 2 MW, 4 MW and 6 MW, respectively. The window center temperature was less than the critical temperature of glass breakage, indicating that the window sprinkler could protect the glass from fire damage well, within the fire scale of 6 MW. The thermal insulation efficiency in the edge region was slightly lower than that in the center of the window. In the range of 2 to 6 MW, there was no significant correlation between the thermal insulation efficiency and the HRR, and the thermal insulation efficiency was in the range of 54% to 59%.

**Keywords:** building fire; fire size; numerical simulation; sprinkler system; glass protection



**Citation:** Gui, J.; Wang, D.; Jiang, Y.; Liu, J.; Yang, L. Study on the Protection Effect of Sprinklers on Glass by Fire Scale in Building Fires. *Fire* **2022**, *5*, 100. <https://doi.org/10.3390/fire5040100>

Academic Editor: Alistair M. S. Smith

Received: 24 April 2022

Accepted: 12 July 2022

Published: 13 July 2022

**Publisher's Note:** MDPI stays neutral with regard to jurisdictional claims in published maps and institutional affiliations.



**Copyright:** © 2022 by the authors. Licensee MDPI, Basel, Switzerland. This article is an open access article distributed under the terms and conditions of the Creative Commons Attribution (CC BY) license (<https://creativecommons.org/licenses/by/4.0/>).

## 1. Introduction

Although glass is widely used in modern architecture, it is easy to break after being heated, which has many potential safety hazards [1–4]. The broken glass not only means that the building structure is damaged, but also that the flame has extra oxygen supply, which leads to the expansion of the scale of the fire [5,6]. When the indoor fire scale increases to a certain extent, the flame will eject out from the building facade, which ignites the heat insulation material [7–9]. Therefore, sprinkler systems are often used in buildings to protect glass from high temperatures and heat radiation [10].

Rahkonen [11,12] proposed that the heat stress caused by temperature difference on the glass surface was the main reason for glass fracture. The heat can be isolated by covering the glass surface with a water film via a sprinkler system, which protects the glass from being damaged [13–15]. Wu et al. [16,17] verified through experiments that a water film could prevent glass from breaking in the event of fire. Richardson [18] found that the radiation heat flow received by the glass surface after being protected by a sprinkler could be reduced by 90% through full-scale experiments. Cai et al. [19] proposed that the water film attenuated the incident heat flow by absorption and scattering. Richardson [20] found that dry spots on the glass surface could be prevented when the water flow rate exceeded 70–90 L/min. In addition, the flow rate of water film had a significant impact on heat insulation [21].

The existence of a sprinkler system will not only weaken the heat radiation received by the glass surface, but also affect the indoor fire evolution [22–24]. Water ejected by a sprinkler absorbs heat through heat radiation and heat convection with flame and smoke. Water can evaporate and absorb heat, and the absorbed heat is equal to the evaporation rate of water multiplied by the latent heat of gasification. Convective heat transfer between water vapor and a gas layer not only changes the temperature balance near the sprinkler, but also the distribution of the gas layer. When the temperature of the gas layer decreases, the heat insulation of the water film and the evolution of the glass surface temperature are also affected. This is a mutual coupling mechanism. Although more reliable glass breakage phenomena and related data can be obtained experimentally, the data that can be obtained experimentally are limited. Numerical simulation is an effective means to obtain a more comprehensive understanding of glass breakage behavior and the evolutionary patterns of key parameters during a fire. Joshi et al. [25] designed a procedure for predicting the breakage behavior and temperature field distribution of glass based on the glass breakage criterion and heat transfer model. Hietaniemi [26] successfully implemented the prediction of the breakage time and surface temperature of glass using the Monte Carlo method. Wang et al. [27,28] used a finite element model to predict the process of crack extension during glass breakage.

Previous studies have focused on the prediction of glass breakage behavior and the protective effect of spraying. However, few researchers have conducted simulation studies on the evolution of glass surface temperature under sprinkler protection. The complex mechanisms of the interaction between sprinkler systems and indoor fires need to be investigated using computational fluid dynamics (CFD) methods. CFD has obvious advantages in the field of the numerical simulation of fires [29–31], and the calculation results can give a comprehensive picture of the development process of indoor fires and the temperature evolution of glass surfaces [32,33]. Moreover, the scale of the fire is a key factor affecting the development of indoor fires and protection effectiveness [34–36]. At different fire scales, the evaporation rate of water and the thermal environment in which the glass is exposed to high temperatures to differ greatly [37]. Therefore, it is necessary to carry out a study of the effect of fire scale on the effectiveness of sprinkler protection. In addition, the correctness of the results of the CFD simulations needs to be verified by full-scale experiments. If the full-scale experiments conducted in this study can verify the correctness of the CFD simulation results, they will provide a more reliable research idea for researchers in related fields. The influence of a sprinkler system on glass surface temperatures and indoor fire evolution under different fire scales can also provide basic theoretical support for fire protection design work.

This paper firstly explains the full-scale experiment of a compartment fire and a window sprinkler protecting the glass to obtain the key characteristic parameters in the fire scene. Then, the full-scale sprinkler experiment is reconstructed by the numerical simulation method, which provides a scientific basis for the in-depth simulation study of the protective cooling effect of a window sprinkler on glass. Finally, the influence of the heat release rate on the protective cooling effect of sprinklers is explored.

## 2. Experimental Design and Numerical Simulation Method

### 2.1. Experimental Design

The experiment was carried out in a full-scale compartment with a length of 5 m, a width of 4.5 m and a height of 3.2 m. The compartment was equipped with a door and a window. The arrangement is shown in Figure 1. The window of the compartment was 1.6 m wide and 1.8 m high, and was equipped with two pieces of tempered glass with a thickness of 8 mm. The size of the door was 1 m wide and 2 m high. The door remained open throughout the experiment. A square pool with an area of  $1 \times 1 \text{ m}^2$  was used as the fire source, and the height of the oil pan was 5 cm. Heptane was used as fuel, and the height of heptane added to the pool was 3 cm in each experiment; the oil pan was placed in the center of the compartment. The experimental conditions are shown in Table 1.

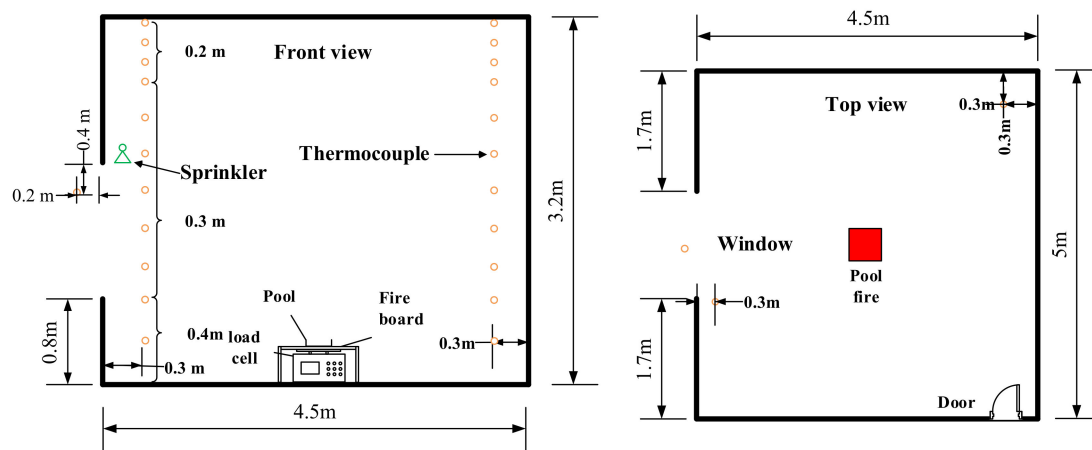


Figure 1. Schematic diagram of the experimental setup.

Table 1. Experimental conditions.

No.	Compartment Size	Glass	Sprinkler System
1	5 m × 4.5 m × 3.2 m	No glass	No sprinkler
2	5 m × 4.5 m × 3.2 m	Two pieces of glass	Window sprinkler

Two rows of thermocouple trees were arranged in the compartment, as shown in Figure 1. Each row of thermocouple trees contained 11 thermocouples, all of which were 0.3 m away from the wall. The bottom thermocouple was 0.4 m from the ground. The temperature changes in the upper part of the compartment were more representative, so thermocouples were more densely arranged in this area. The distance between the two thermocouples at the bottom was 0.4 m, and the distance between the four thermocouples at the top was 0.2 m. A thermocouple was placed outside the window to monitor the outdoor temperature change. The thermocouple was located in the middle of the window, with a horizontal distance of 0.2 m from the window and 0.4 m from the upper edge of the window. The distance between thermocouples in the middle was 0.3 m.

Sprinkler systems to protect building elements in a fire are a very efficient and widely proven method [29,30]. The horizontal distance between the sprinkler and the top of the glass was 0.2 m. The operating pressure of the sprinkler was controlled by a valve on the pipeline. The window sprinkler used in the experiment, as shown in Figure 2, had a working pressure of 0.1 MPa. The window sprinkler was a special model used to protect building components such as window glass or glass curtain walls. The K coefficient of the window sprinkler was 63.5, the diameter of the glass bubble was 3 mm and the response temperature was 68 °C. Once the sprinkler was started, it would continue to spray water until the end of the experiment. The accumulated water generated in the experimental compartment was discharged out of the compartment through a ditch on the ground.



Figure 2. Window sprinkler.

## 2.2. Numerical Simulation

FDS is one of the most professional types of CFD simulation software and has been widely used in fire numerical research, which has the characteristics of few assumptions and small error of results. The default operation of FDS is a large eddy numerical simulation. Similar to other software for computational fluid dynamics, the FDS fluid dynamics model is a numerical model of the Navier–Stokes equations (N-S equations) that can be used to simulate combustion processes at low Mach numbers. The basic control equations are as follows:

- (1) Component transport equation

$$\frac{\partial}{\partial t}(\rho Y_i) + \nabla \cdot \rho Y_i u = \nabla \cdot \rho D_i \nabla Y_i + \dot{m}_i''' \quad (1)$$

where  $Y_i$  is the mass fraction of component  $i$ ;  $D_i$  is the diffusion fraction of the component  $\text{m}^2/\text{s}$ ; and  $\dot{m}_i'''$  is the unit mass generation rate,  $\text{kg}/(\text{m}^3 \cdot \text{s})$ .

- (2) Mass conservation equation

$$\frac{\partial \rho}{\partial t} + \nabla \cdot \rho u = 0 \quad (2)$$

where  $\rho$  is the gas density,  $\text{kg}/\text{m}^3$ ;  $t$  is the fire simulation time,  $\text{s}$ ; and  $u$  is the gas velocity,  $\text{m}/\text{s}$ .

- (3) Momentum conservation equation

$$\frac{\partial}{\partial t}(\rho u) + \nabla \cdot \rho u u + \nabla p = \rho f + \nabla \cdot \tau_{ij} \quad (3)$$

where  $p$  is the mixed gas pressure,  $\text{Pa}$ ;  $f$  is the external pressure,  $\text{Pa}$ ; and  $\tau_{ij}$  is the viscosity,  $\text{Pa} \cdot \text{s}$ .

- (4) Energy conservation equation

$$\frac{\partial}{\partial t}(\rho h) + \nabla \cdot \rho h u = \frac{Dp}{Dt} + \dot{q}''' - \nabla \cdot q + \varphi \quad (4)$$

where  $h$  is the enthalpy of the gas component,  $\text{kJ}/\text{kg}$ ;  $\dot{q}'''$  is the heat release rate,  $\text{kW}/\text{m}^3$ ;  $q$  denotes the radiant heat,  $\text{kW}/\text{m}^2$ ; and  $\varphi$  denotes the dissipation rate,  $\text{kW}/\text{m}^3$ . In FDS, the partial differential equations in the above conservation equations are approximated as finite differences and solved in real time by a divided 3D mesh [31].

In order to prove the effectiveness of the sprinkler simulation by comparing the simulation results with the full-scale experimental results, the physical model of numerical simulation was built with reference to the experimental combustion compartment, as shown in Figure 3. The model size of the combustion compartment was  $4.5 \text{ m} \times 5.0 \text{ m} \times 3.2 \text{ m}$  and the left wall was equipped with a glass window with a size of  $1.8 \text{ m} \times 1.6 \text{ m}$ . A door of  $1.0 \text{ m} \times 2.0 \text{ m}$  was opened in the front wall reference experimental setting. Concrete and glass were used in the model, and the material setting parameters are shown in Table 2.

The main boundary conditions are as follows.

$$T_\infty = 293 \text{ K}$$

$$\rho_\infty = 1.2 \text{ kg}/\text{m}^3$$

$$c_p = 1.0 \text{ kJ}/(\text{kg} \cdot \text{K})$$

$$g = 9.81 \text{ m}/\text{s}^2$$

$$P_\infty = 0.1 \text{ MPa}$$

$$V_{\infty} = 0 \text{ m/s}$$

$$T_w = 293 \text{ K}$$

where  $T_{\infty}$  is the ambient temperature,  $\rho_{\infty}$  is the air density,  $c_p$  is the specific heat at constant pressure of the air,  $g$  is the acceleration of gravity,  $P_{\infty}$  is the normal atmosphere,  $V_{\infty}$  is the ambient wind velocity and  $T_w$  is the temperature of the compartment walls.

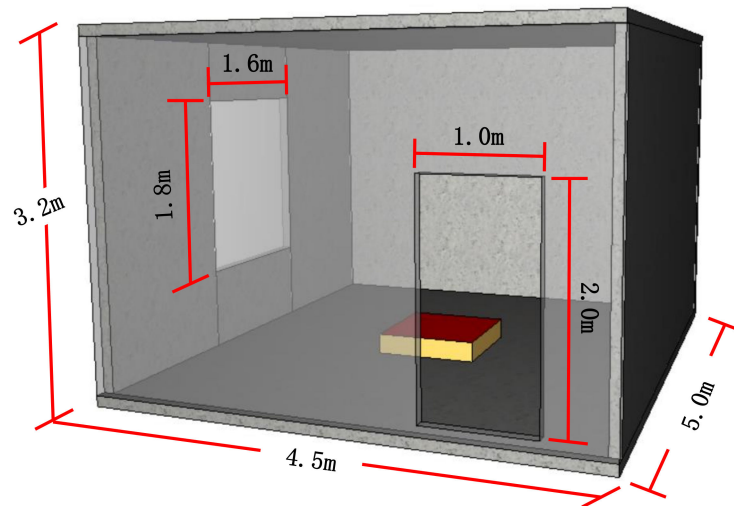
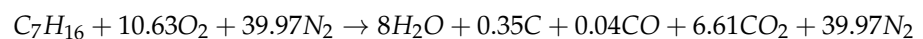


**Figure 3.** Physical model of the combustion compartment.

**Table 2.** Thermal physical parameter settings for glass [25,26].

Material Name	Density (kg/m <sup>3</sup> )	Specific Heat (kJ/(kg·K))	Heat Conductivity (W/(m·K))	Emissivity
Glass	2700.0	0.837	1.4	0.86
Concrete	2280	1.04	1.8	0.92

In the simulations, the fuel was chosen as n-heptane as in the full-scale experiments. The yields of carbon monoxide and soot during the n-heptane combustion were 0.012 and 0.042 [32], respectively. Therefore, the combustion reaction of n-heptane was set to:



The combustion heat of n-heptane is 48 MJ/kg.

In order to obtain the change of temperature field under the sprinkler, two groups of thermocouple trees were set up, and their arrangement is shown in Figure 4. Thermocouple tree 1 was set 0.4 m away from the horizontal direction of the window and was used to detect the change of the longitudinal temperature field near the window after the sprinkler was turned on, so as to judge the protective effect of the sprinkler spraying on the window. Thermocouple tree 2 was arranged in the corner of the compartment to monitor the temperature change far away from the fire source during fire extinguishing.

Window sprinklers were used in the simulation. The flow coefficient (K) of the window sprinkler was 63.5, the operating pressure was 0.1 MPa and the response temperature was 68 °C. The initial velocity of the droplets was 6 m/s, the spraying angle was 90.0°, and the median diameter of each droplet was 550 μm. The FDS can simulate the droplet distribution based on the basic parameters of the nozzle.

A reasonable mesh size is the premise to ensure the reliability of the simulation results, so mesh independence analysis is needed [36–38]. According to the calculation, the mesh size should be selected in the range of 0.0889 to 0.3556. Four mesh size setting options are selected for mesh independence analysis, as shown in Table 3.

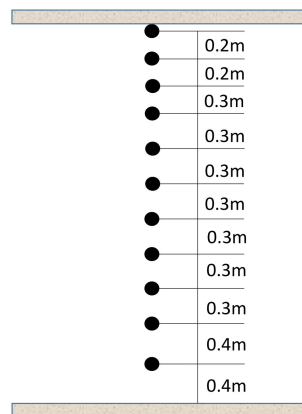


Figure 4. Arrangement of the thermocouple trees.

Table 3. Mesh size setting options.

Mesh Size Setting	X-Axis Mesh Size (m)	Y-Axis Mesh Size (m)	Z-Axis Mesh Size (m)
1	0.2531	0.2514	0.2556
2	0.2025	0.2000	0.2000
3	0.1000	0.1000	0.1000
4	0.0800	0.0800	0.0807

Figure 5 is the trend chart of the heat release rate under different mesh size settings. It can be seen that the curve coincidence degree of the heat release rate and temperature gradually increases with the decrease of the mesh size. When the mesh size is less than 0.1 m, the mesh size has little effect on the heat release rate. Therefore, the mesh size setting mode of 3 is selected in order to give consideration to both simulation accuracy and operation cost.

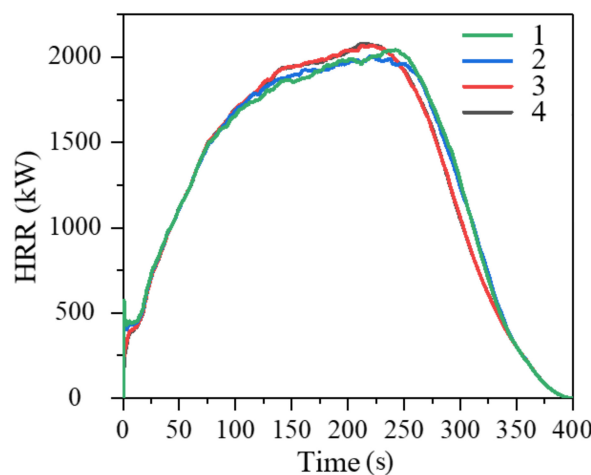
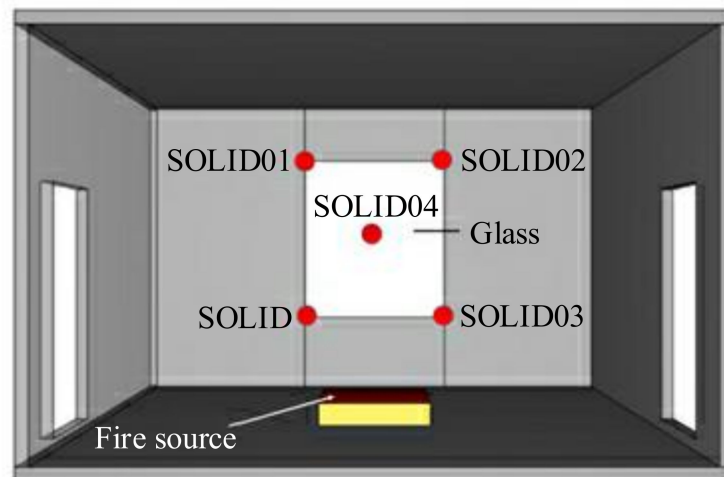


Figure 5. Heat release rate trend chart for different mesh settings.

The three heat release rates are 2, 4 and 6 MW, respectively, which represent different fire scenarios. The fire scene is analyzed and the glass surface temperature, incident heat flux and water film insulation efficiency are compared to reveal the best conditions for the glass protective effect under different fire conditions. The temperature of glass is an important basis for judging the protective effect of a window sprinkler. The research of Skelly et al. [22] showed that when the temperature difference between the center and the

edge of a glass pane exceeded  $90\text{ }^{\circ}\text{C}$ , the glass would break. In order to explore whether the temperature difference between the center and the edge of glass under a window sprinkler meets the critical requirement of cracking and to quantify the protection degree of a window sprinkler for glass, five solid surface temperature detection devices were set at the four corners and the center of the window to detect the temperature gradient of the window surface; these devices are named SOLID, SOLID01, SOLID02, SOLID03 and SOLID04, respectively. Their specific arrangement is shown in Figure 6. In addition, other monitoring devices were provided at the same location for monitoring the incident heat flux, radiant heat flux and convective heat flux.

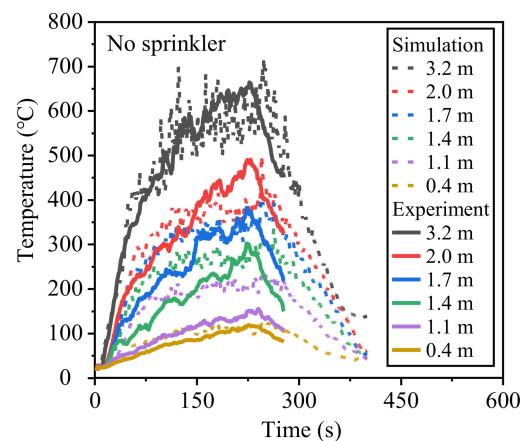


**Figure 6.** Layout of the temperature monitoring equipment.

### 3. Results and Discussion

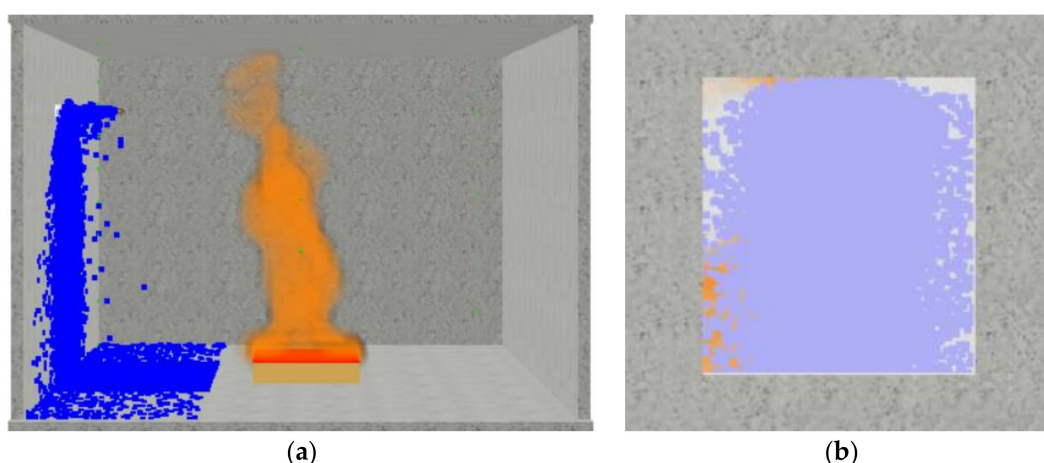
#### 3.1. Verification of Numerical Simulation Results

It is necessary to verify the results of the numerical simulation before using the simulation results for discussion. Figure 7 compares the full-scale experimental temperature with the numerical simulation temperature. The simulated values of the window temperature are in good agreement with the experimental values. Especially at the height of 3.2 m, the temperature curve shows a very high degree of fitting in the development and steady-state stage, which shows that the simulation results reduce the influence of the gas layer on the temperature well.



**Figure 7.** Comparison of window edge temperatures between the simulation and experiment under the non-sprinkler condition.

The simulation results of the window sprinkler protection experiment under 0.1 MPa working pressure are shown in Figure 8a. The droplets were sprayed by the window sprinkler continuously and covered the glass surface evenly to form a water film protective layer. No droplets entered the pool, which is consistent with the experimental phenomenon. As can be seen from Figure 8b, when the installation height of the sprinkler is consistent with the upper edge of the window, the sprinkler droplets can cover almost the whole window, and only the small areas above the left and right edges cannot be covered due to the influence of gravity. In the aspect of water film thickness, the water film protective layer formed by the window sprinkler on glass is uniform in thickness and has good protective effect.



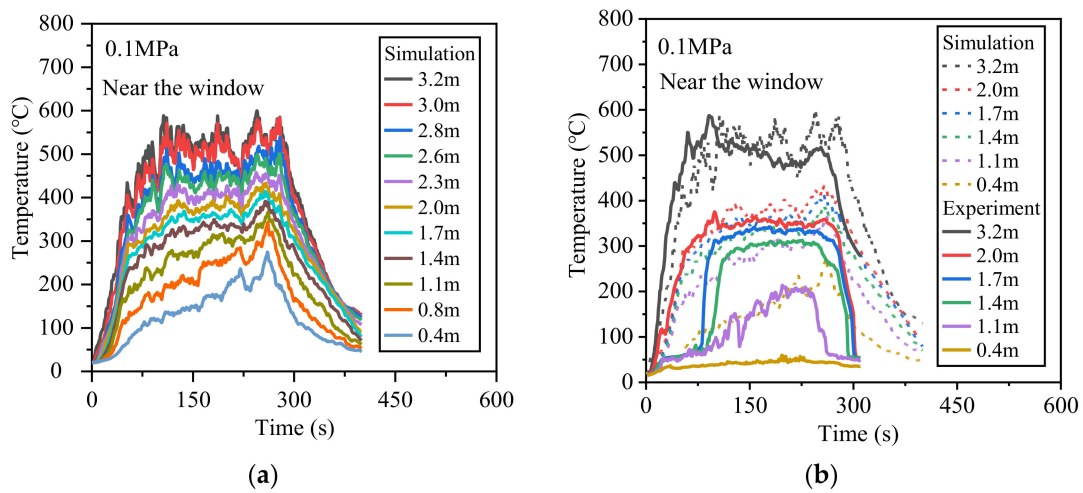
**Figure 8.** Window sprinkler protection experiment with a working pressure of 0.1 MPa: (a) sprinkler form, (b) window glass protective effect.

Figure 9a shows the simulation results of the window edge temperature when a window sprinkler protects glass. The hot gas in the protection area of the window sprinkler is affected by the droplet drag force and settles downward, compared with the non-sprinkler condition. The gradient of the temperature drop in the compartment is obviously reduced. For example, as shown in Figure 9b, when the height is greater than 2 m, the simulated values show a very high degree of agreement with the experimental values in both the development and steady-state stage. For the area with a height below 2 m, because of the influence of the sprinkler on the thermocouple, the experimental value shows a time lag in the development stage. In the steady-state stage, the simulated values and experimental values still show a high degree of reduction, which shows that the FDS numerical model and the selection of boundary conditions are reliable for steady-state simulation.

Figure 10a shows the simulation results of the compartment's interior temperature. It is worth noting that the temperature gradient between 0.4 m and 0.8 m is relatively large. This is because the thermocouple is located below the door at 0.4 m, and cold air flows to the compartment from below the door, so the temperature at 0.4 m is lower. The comparison of the experimental and simulation results is shown in Figure 10b. The simulation results at the top of the compartment are in the highest agreement with the experimental values, while the simulation values at the bottom of the compartment are slightly higher than the experimental values; however, the overall development trend is very close.

### 3.2. Fire Evolution

The characteristic parameters such as the temperature of the glass surface before and after the sprinkler activation have different evolutionary trends at different fire sizes. Therefore, this section will present the evolution of parameters such as glass surface temperature for indoor heat release rates of 2, 4 and 6 MW, respectively.



**Figure 9.** Window sprinkler protection experiment window edge temperature at 0.1 MPa operating Pressure: (a) simulation value, (b) comparison with experimental value.

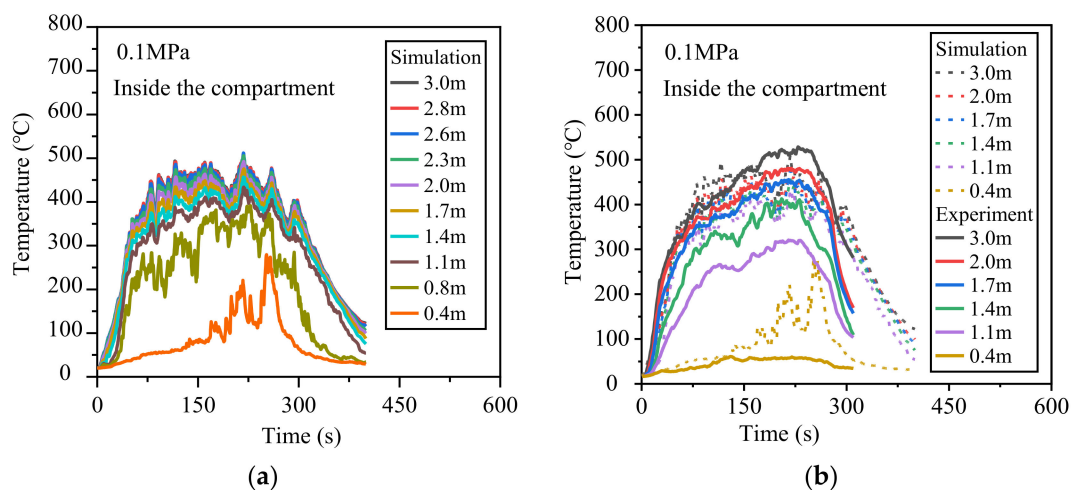


**Figure 10.** Window sprinkler protection experiment internal temperature at 0.1 MPa operating pressure: (a) simulation value, (b) comparison with experiment value.

When the HRR of the fire source is 2 MW, the temperature of the window glass surface changes with time before and after starting the window sprinkler, as shown in Figure 11. The surface temperature of the glass gradually increases with time before the sprinkler is started. The highest temperature in the middle of glass reaches 85 °C, which exceeds the temperature in any other corner. The main reason for this phenomenon is that when the power of the fire source is 2 MW, the height of the fire source is low, the width is narrow and the amount of smoke generated is less, so the thickness of the smoke layer accumulated above the space is low, which leads to weak convective heat transfer at the upper edge of the glass. The smoke particles in the smoke layer will block the heat radiation of the flame and reduce the heating of the glass, so the temperature in the middle of the glass is relatively high. When the sprinkler is started, the temperature in the corner of the upper edge of the glass is less affected by the sprinkler, while the temperature in other positions begins to drop after being sprayed for 50 s and the temperature in the middle position drops most obviously. This is because the window sprinkler in the middle position of the water sprinkler intensity is the highest; the formation of the water film’s protective effect is the best. The results show that the window sprinkler has good heat dissipation and heat radiation isolation. The highest temperature in the middle and lower corners of the glass

is controlled within 50 °C under the protection of a window sprinkler, and the highest temperature difference is less than 20 °C.

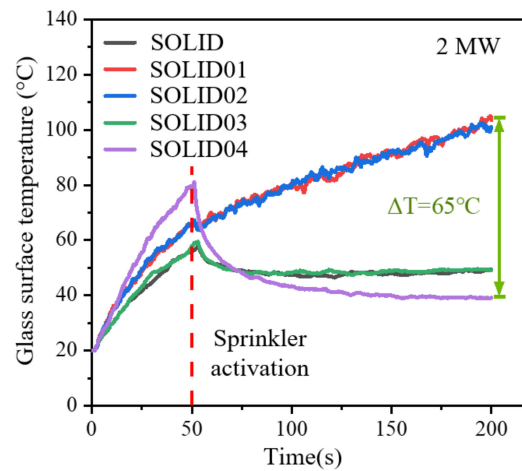


**Figure 11.** Glass surface temperature change under window sprinkler conditions.

The temperature field can reflect the whole change process of the glass surface temperature more intuitively. As shown in Figure 12a, the temperature distribution on the window glass surface decreases radially from the middle of the upper edge to the outer edge when the 50 s sprinkler is started, which is mainly affected by the combined action of the smoke layer and fire source radiation. Figure 12b shows the temperature field of the glass surface for 150 s; the sprinkler intensity in the center of the window sprinkler is the highest and the protective effect is the best after the sprinkler has been started. The temperature drop on the center line of the glass is the most obvious, while the temperature in the corners on both sides of the upper edge has continuously increased over 100 °C due to the blind area of the sprinkler.

The fine particles contained in the gas layer can absorb the heat radiation of the fire source during combustion. The distribution of the gas layer in the combustion compartment, shown in Figure 13a,b, are after 50 s and 150 s of spraying, respectively. According to the simulation results of Figure 14, the height of the smoke layer above the compartment is about 3–3.2 m when the power of the fire source is 2 MW and the smoke layer is thin. At 50 s, the window sprinkler starts to operate; the sprinkler droplets at low temperature reduce the temperature of the gas and have a certain drag force to make the gas sink. In addition, the limited air supply on the right side causes the flame to tilt.

Figure 15 shows the change of glass exposed to heat radiation from a fire source. After the fire, the heat radiation received by the glass surface increased rapidly and approached the steady state in 25 s. The maximum radiant heat flux appears in the center of the window, and the maximum value is about 16 kW/m<sup>2</sup>. This is because the flame height is lower and the width is narrower when the power of the fire source is 2 MW, and the radiant heat flux at the middle position of the glass closest to the fire source is greater. The soot particles in the smoke layer have a certain shielding effect on the radiation of the fire source and also reduce the influence of radiation on the glass. With the start of sprinkler, the radiant heat flux drops sharply at 50 s and tends to be stable at 60 s. The heat radiation in the middle position decreased the most, reaching about 62%. Spraying droplets form a water film on the glass surface, and both the water film and the water vapor layer formed by the evaporation of droplets have the function of attenuating flame radiation.

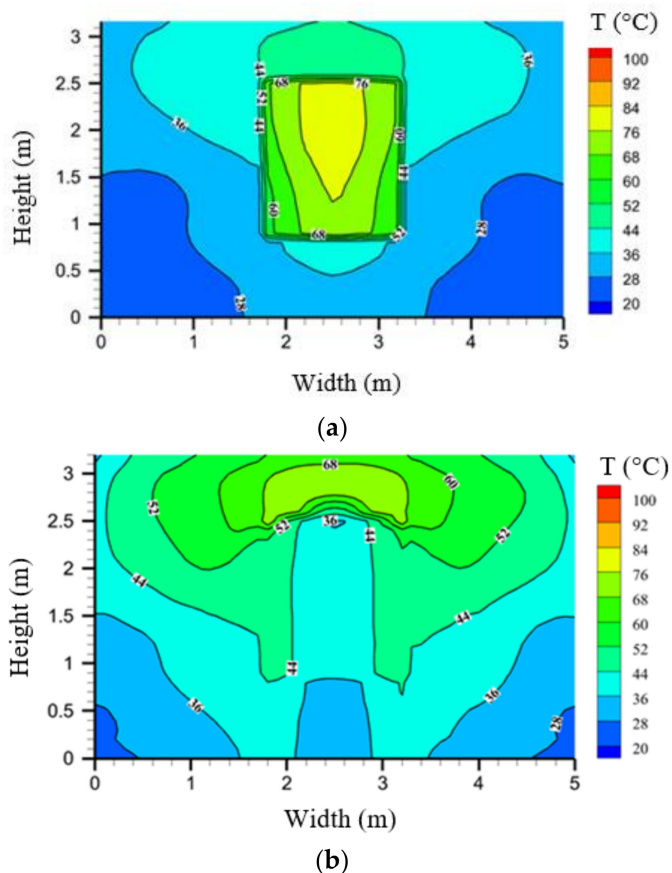


Figure 12. Temperature field of the glass surface under window sprinkler conditions: (a) 50 s, (b) 150 s.

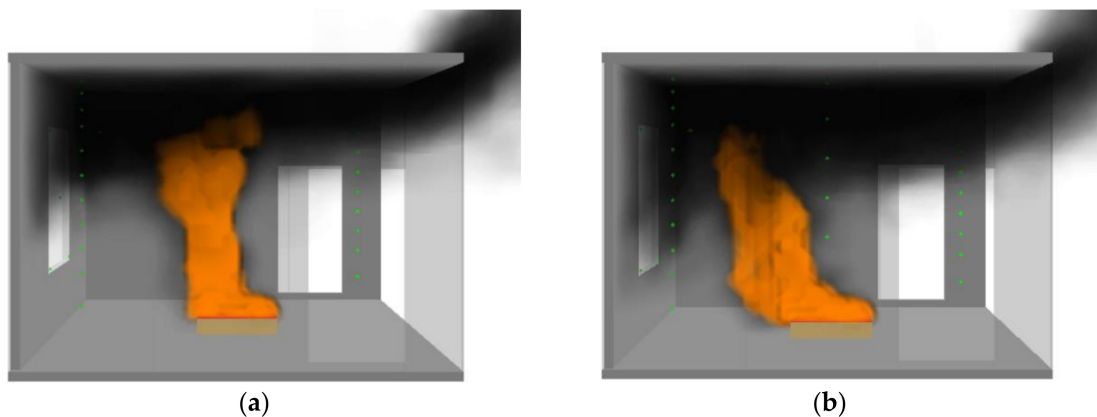


Figure 13. Smoke distribution under window sprinkler conditions: (a) 50 s, (b) 150 s.

Different from the radiant heat flux, as shown by the convective heat flux curves at different positions of the window glass in Figure 16, the convective heat transfer in different areas of the window glass before and after the start of the window sprinkler shows a positive correlation with the height. This is because convective heat transfer depends on the temperature difference between the window and environmental temperature. According to Figure 16, the higher the height, the higher the environmental temperature, the greater the temperature difference between the glass and the environmental temperature and the stronger the convective heat transfer, and the convective heat flux at the upper edge of the glass reaches  $3.0 \text{ kW/m}^2$ . When the height is lower than 1.7 m, the environmental

temperature is lower and the convective heat transfer is greater. The convective heat flux under the glass is almost zero.

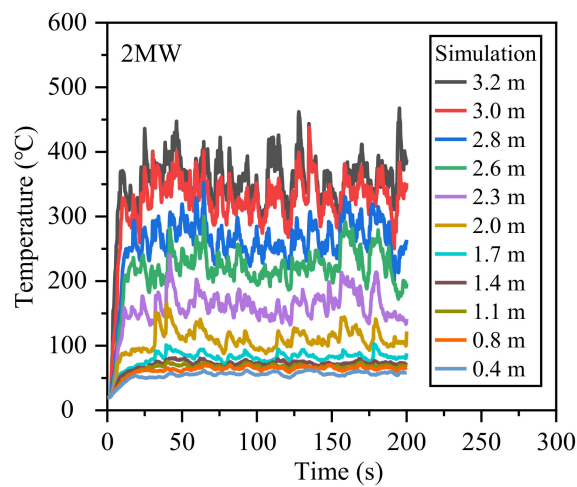


Figure 14. Window edge temperature under window sprinkler conditions.

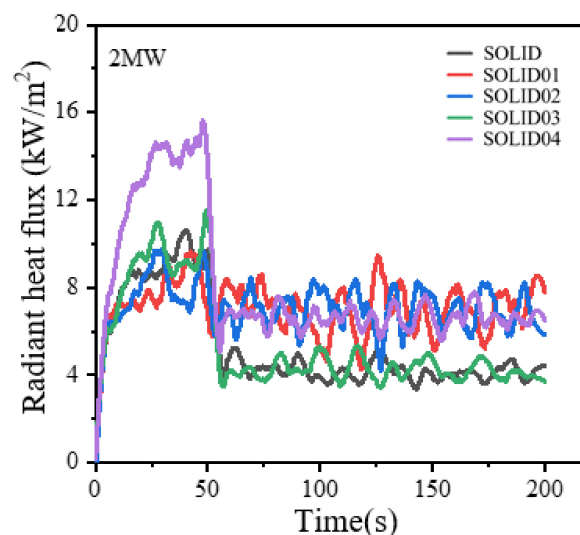
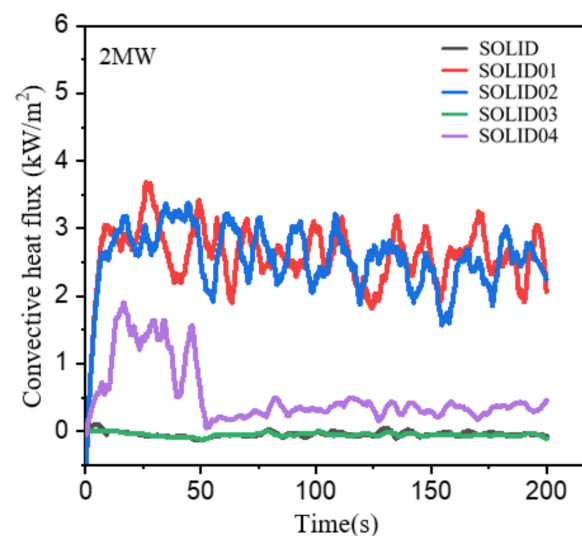


Figure 15. Glass radiant flux variation under window sprinkler conditions.

Figure 17 is the curve of the incident heat flux at different positions on the window glass. The radiant heat flux received by the window is much larger than the convective heat flux, and the variation law of the incident heat flux is consistent with that of the radiant heat flux, which shows that the heat radiation from the fire source is the main reason for the temperature rise of the window.

When the power of the fire source is 4 MW, the temperature of the window glass surface changes with time before and after starting the window sprinkler, as shown in Figure 18. Before the sprinkler was started, the surface temperature of the glass gradually increased with time and the top edge temperature of the glass reached 150 °C, which was slightly higher than the center temperature of the glass. The lower edge temperature of the glass is obviously low; the highest is only 80 °C and the temperature difference of the whole glass is 70 °C. Compared with the simulation results of a 2 MW power source, the temperature of the upper edge of the glass rises significantly, mainly because the height of the fire source reaches the ceiling when the fire source power is 4 MW, forming a transverse ceiling spray, releasing more high-temperature gas and accumulating a thick gas layer

above the compartment. When the sprinkler is started, the temperature at the corner of the upper edge of the glass is less affected by the sprinkler, and the temperature will continue to rise to 250 °C. The glass surface temperature at other positions began to drop 50 s after the sprinkler was started. Among them, the center position of the window dropped most obviously, from 142.2 °C before the sprinkler to 58.6 °C at the end, with a drop range of 59%. This is consistent with the simulation results of a 2 MW fire with a window sprinkler. The results show that when the power of the fire source is 4 MW, the window sprinkler still has a good function of heat dissipation and heat radiation isolation. Under the protection of a window sprinkler, the highest temperature of the middle and lower edge of the glass is controlled within 70 °C and no cracking will occur.



**Figure 16.** Variation of convective heat flux of glass under window sprinkler conditions.

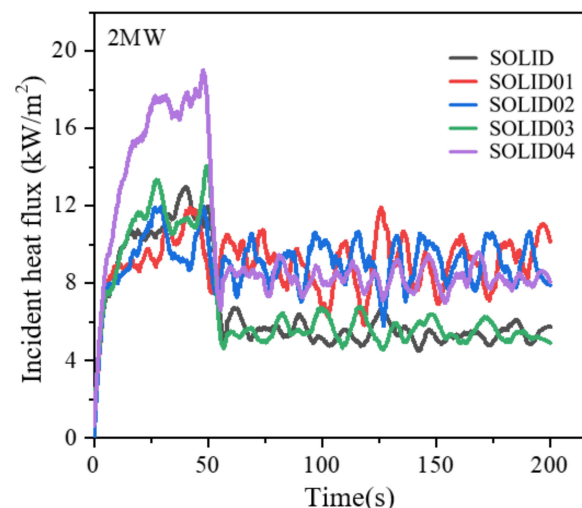


**Figure 17.** Glass incident heat flux variation under window sprinkler conditions.

The following analysis of the temperature field shows the overall change process of the glass surface temperature more intuitively. As shown in Figure 19a, the temperature field on the surface of the window glass shows a high-temperature trend at the top and center and a low-temperature trend at the bottom when the 50 s sprinkler has just been started. Among them, the surface temperature of the glass above the window is the highest, reaching 150 °C. This distribution trend is formed by the combined action of fire source radiation and the smoke layer. The flame height increases, the fire radiation above the window increases

and the high temperature smoke layer accumulated above the compartment makes the surface temperature of the glass above the window the highest. The center of the window is less affected by the smoke layer, and the surface temperature is slightly lower than that of the upper glass. Figure 19b is the temperature field of a glass surface for 150 s. The sprinkler intensity in the center of the window sprinkler after the sprinkler was started is the highest and the protective effect is the best. The temperature on the center line of the glass drops most obviously, dropping below 50 °C in 150 s. However, the temperature of the two corners of the upper edge rises to nearly 150 °C continuously because the corners are in the blind area of the sprinkler, which is similar to the simulation results of the 2 MW window sprinkler.

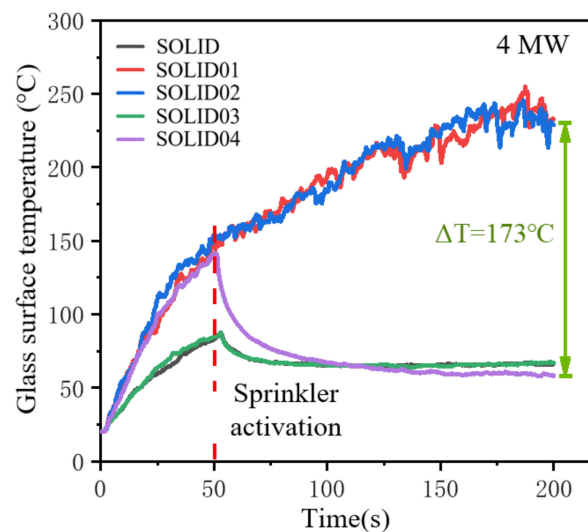


**Figure 18.** Glass surface temperature change under window sprinkler conditions.

Figure 20a,b are 50 s and 150 s, respectively. According to the simulation results of Figure 21, when the HRR is 4 MW, the window temperature is obviously higher than that when the HRR is 2 MW, and the increment is about 200 °C. The height of the gas layer above the compartment is about 2.8–3.2 m, and the thickness of the gas layer increases. With the start of the window sprinkler in 50 s, the low-temperature sprinkler droplets cool the environmental temperature and have a certain drag force which makes the smoke sink; the ambient air supply is limited, and the flame inclines.

Figure 22 shows the change of the heat radiation of the fire source to the glass before and after the application of the window sprinkler. After ignition, the heat radiation received by the glass surface increases rapidly and approaches a steady state in 25 s. The radiant heat flux received by the upper edge of the window is close to the center of the window and obviously higher than that at the lower edge of the window, with a maximum difference of 20 kW/m<sup>2</sup>. With the sprinkler's start, the radiant heat flux of each position of the window glass drops sharply, and tends to be stable at about 60 s. Under the action of the sprinkler, the heat radiation in the center of the window decreased the most, from 29.2 kW/m<sup>2</sup> to 12.1 kW/m<sup>2</sup>, with a decrease range of about 60%. This is because droplets form a water film on the glass surface, and both the water film and the water vapor layer formed by droplet evaporation have the function of attenuating flame radiation; their attenuation effect on radiation depends on the thickness of the water film, so the water film at the center of the window is the thickest and the attenuation effect is the strongest. Because the upper edge of the window is in the sprinkler's blind area, the reduction of heat radiation is not obvious.

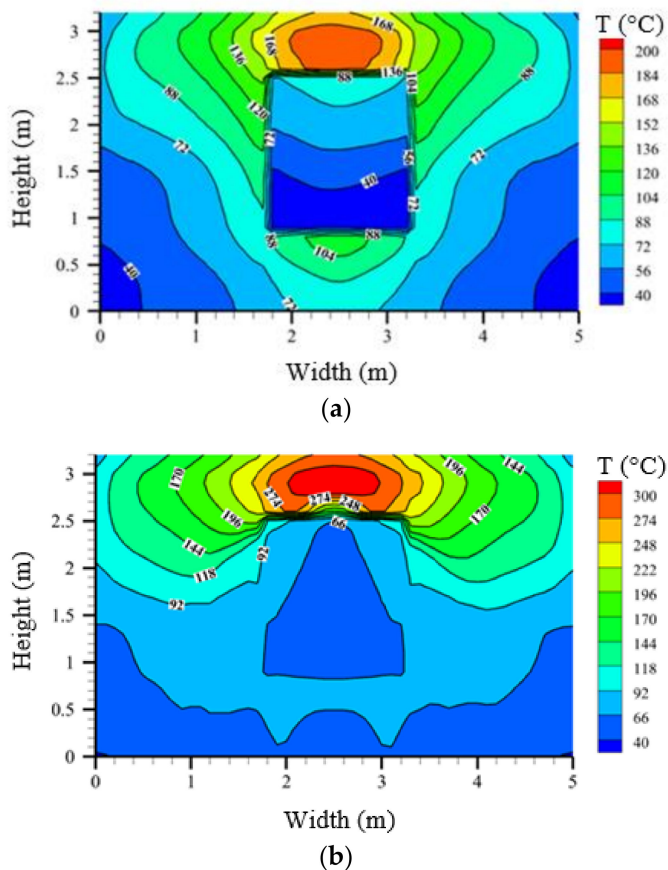


Figure 19. Temperature field of glass surface under window sprinkler conditions: (a) 50 s, (b) 150 s.

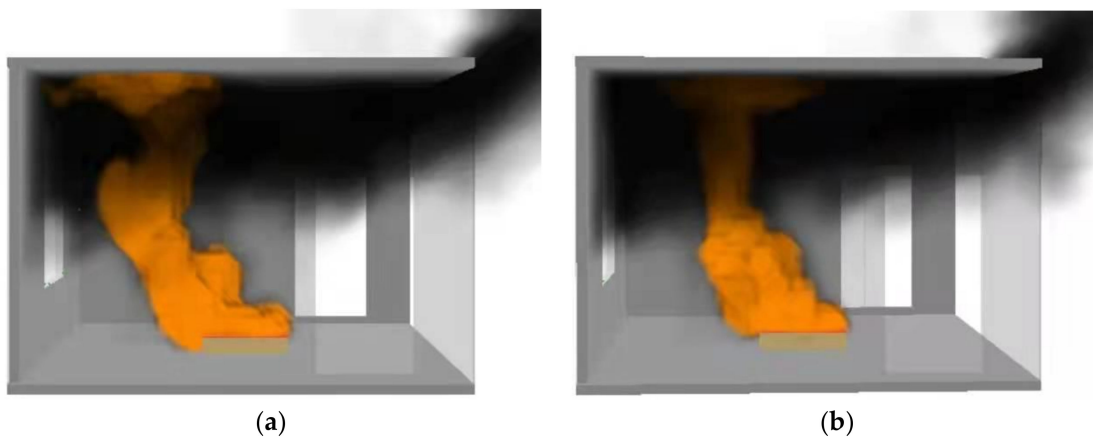


Figure 20. Smoke distribution under the action of a window sprinkler: (a) 50 s, (b) 150 s.

Figure 23 is the convection heat flux curve at different positions on the window glass in the simulation of a 4 MW window sprinkler. Similar to the simulation results of the 2 MW window sprinkler, the convective heat transfer in different areas of the glass shows a positive correlation with height before and after the window sprinkler has been started. The higher the height, the higher the environmental temperature, the greater the temperature difference between the glass and the environmental temperature and the stronger the convective heat transfer, and the convective heat flux at the upper edge of the glass reaches  $6.0 \text{ kW/m}^2$ . When the height is lower than 1.7 m, the environmental temperature is lower and the convective heat transfer is weaker. The convective heat flux under the glass

is almost zero. With the start of the sprinkler, the convective heat flux in the center of the window decreased rapidly and most obviously, from  $2.8 \text{ kW/m}^2$  before the start to  $0.5 \text{ kW/m}^2$  with a decrease of 82%. This is mainly due to the cooling effect of the sprinkler droplets' vaporization, which makes the environmental temperature around the window center decrease and the convective heat transfer weaken.

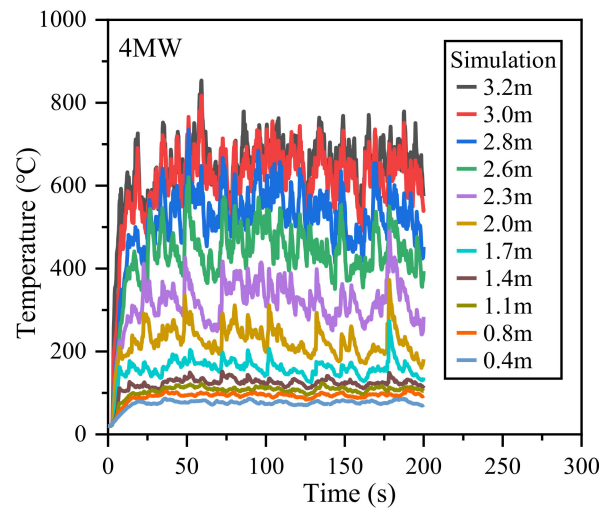


Figure 21. Window edge temperature under window sprinkler conditions.

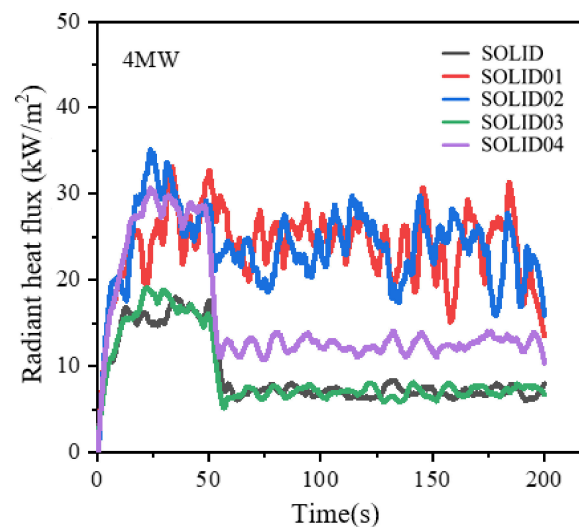
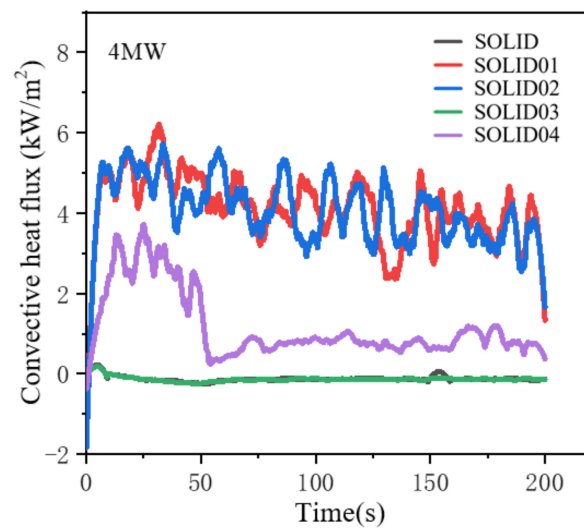
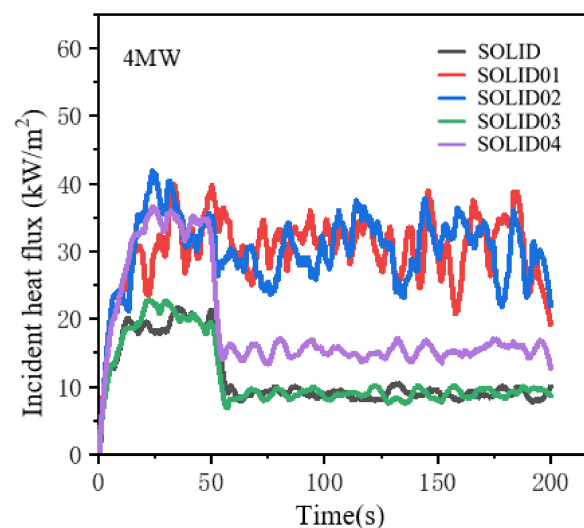


Figure 22. Glass radiant heat flux variation under window sprinkler conditions.

Figure 24 is the curve of the incident heat flux at different positions on the window glass, and the incident heat flux at different positions on the window glass still shows the same change rule as the radiant heat flux. The incident heat flux in the window's center is most affected by the sprinkler and its value drops rapidly from  $34.7 \text{ kW/m}^2$  to  $14.3 \text{ kW/m}^2$  with the sprinkler start-up, with a decrease of 59%. Because the upper edge of the window is not covered by sprinkler droplets, its incident heat flux is not significantly affected.



**Figure 23.** Variation of convective heat flux of glass under window sprinkler conditions.



**Figure 24.** Glass incident heat flux variation under window sprinkler conditions.

The surface temperature of the glass when the heat release rate of the fire source is 6 MW is shown in Figure 25. The temperature in the lower left, lower right and center is on an upward trend in the range of 0–50 s. The temperature in the lower left and lower right reaches the highest point of 105.7 °C in 50 s, and the center temperature reaches the highest point of 186.7 °C in 50 s. In the range of 51–200 s, the temperature slowly drops to 74.6 °C. This is because the window sprinkler starts at 50 s, the sprinkler forms a water curtain to cover the window and the temperature in the lower left, lower right and center begins to decrease. Because the temperature measuring point in the center is 0.85 m higher than that in the lower part, it is relatively less affected by water flow and the temperature is higher than that in the lower part. The temperature in the upper left and upper right has been on the rise, with the highest temperature reaching 375.8 °C and the maximum temperature difference from the lower and central positions being 300 °C. This is because the sprinkler and the upper measuring point are located at 2.6 m from the upper edge of the window, so there is basically no cooling effect of the water flow above the glass. Through the lower left, lower right and center glass surface temperature curves, it can be concluded that the window sprinkler has a cooling effect on the glass surface, which can effectively protect the safety of glass.

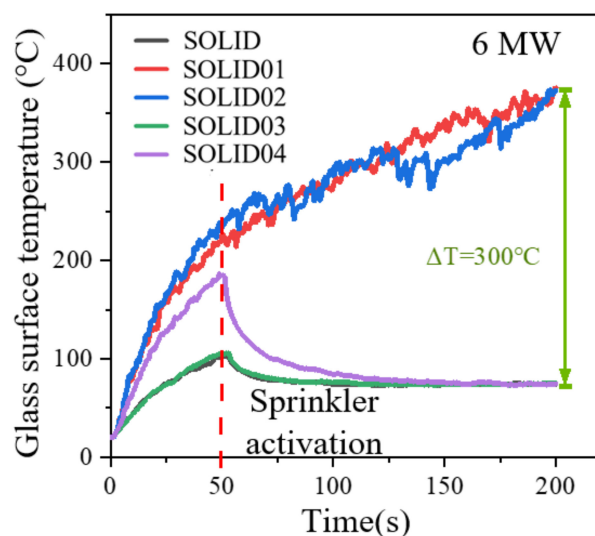


**Figure 25.** Glass surface temperature change under window sprinkler conditions.

Figure 26a is the temperature distribution of the glass surface temperature field at 50 s. It can be seen from the figure that the temperature above the compartment is higher than that below, which is due to the high power of the fire source. With the combustion reaction, the flame height rises and the flame diffuses upward, resulting in the higher temperature above. The temperature in the glass area is higher than the environmental temperature and the long-term high temperature poses a serious threat to the safety of glass, so the sprinkler is set to start at 50 s. Figure 26b shows the temperature distribution of the glass surface temperature field at 150 s. It can be seen from the figure that after 100 s after the window sprinkler has been started, the temperature under and in the middle of the glass surface is obviously weakened compared with that at 50 s, which is almost the same as the surrounding temperature. Because the water flow of the window sprinkler is basically not covered, the temperature change is not obvious.

Figure 27a,b are the smoke layer distribution of the simulated fire scene at 50 s and 150 s, respectively. It can be seen from the window-side simulation diagram in Figure 28 that when the HRR is 6 MW, the window-side temperature also increases with the increase of height and the window-side temperature increases significantly from 100–200 °C, compared with the 2 MW and 4 MW conditions. The smoke layer of the compartment is 2.5–3.2 m and the thickness of the smoke layer of the lower power fire source has increased. It can be seen from the figure that the fire has a decreasing trend compared with the 50 s, and there is no large area of flame coverage on the top of the compartment. With the progress of the combustion reaction, the thickness of the smoke layer has an upward trend, indicating that the start of the sprinkler has slowed down the further expansion of the fire and increased the safety of the glass.

The radiative heat flux simulated by the 6 MW window sprinkler is shown in Figure 29. The radiative heat fluxes in the lower left, lower right and center rise to the steady-state stage in the range of 0–50 s, and the radiative heat fluxes in the steady-state stage are 20.9 kW/m<sup>2</sup>, 21.7 kW/m<sup>2</sup> and 38.8 kW/m<sup>2</sup>, respectively, dropping to 9.5 kW/m<sup>2</sup>, 9.7 kW/m<sup>2</sup> and 16.5 kW/m<sup>2</sup> at 50–200 s. The radiant heat flux of the upper left and upper right parts is in the fluctuation range of 30–50 kW/m<sup>2</sup> due to air supplementation. Therefore, the window sprinkler has a significant weakening effect on the radiant heat flux below and in the middle of the glass, but has no obvious effect on the upper measuring points at the same height.

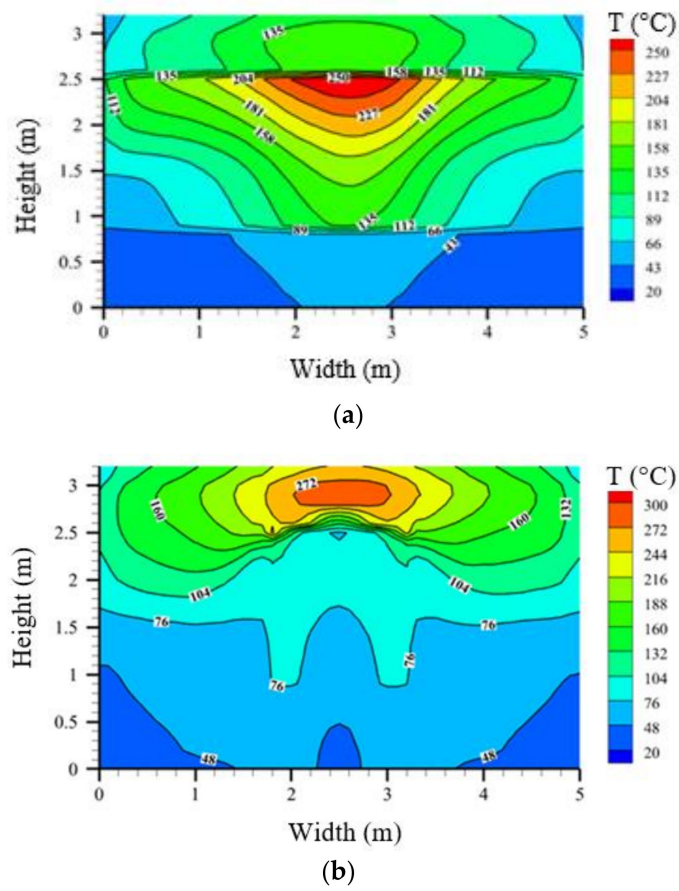


Figure 26. Temperature field of glass surface under window sprinkler conditions: (a) 50 s, (b) 150 s.

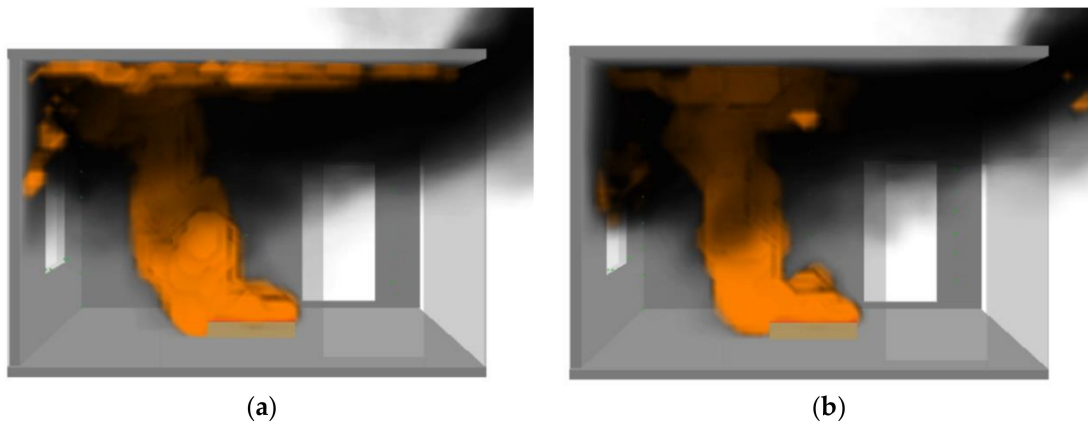


Figure 27. Gas distribution under window sprinkler conditions: (a) 50 s, (b) 150 s.

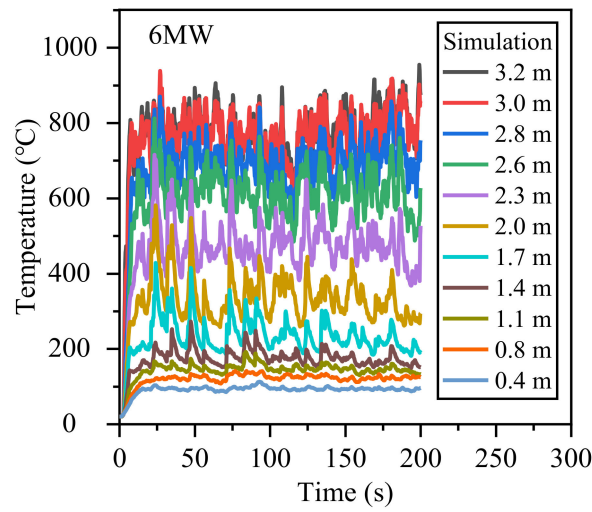


Figure 28. Window edge temperature under window sprinkler conditions.

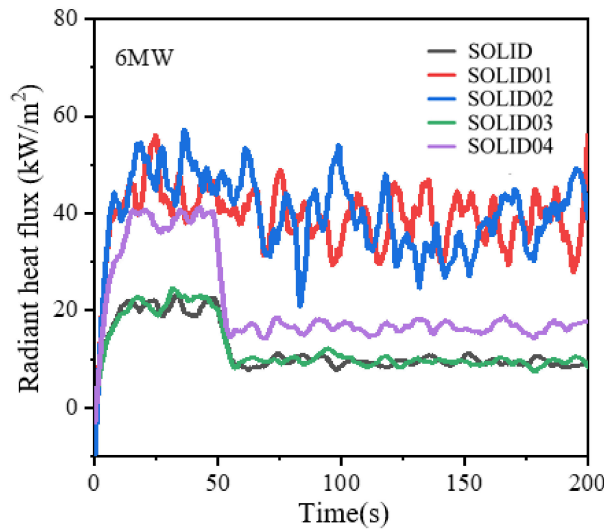


Figure 29. Variation of radiant heat flux of glass under window sprinkler conditions.

The convective heat flux simulated by the 6 MW window sprinkler is shown in Figure 30. The convective heat fluxes in the lower left and right are essentially zero throughout the simulation, because the temperature difference between the underside of the glass and the environmental temperature is small, and there is essentially no convective heat transfer between the two. The convective heat fluxes in the center, upper left and upper right first increased and then decreased during 0–200 s, because before the sprinkler was not started, due to the progress of the combustion reaction, the temperature difference between the temperature in the center, upper left and upper right of the glass and the environmental temperature gradually increased, so the convective heat flux shows an upward trend before 50 s. When the window sprinkler is activated at 50 s, the temperature in the middle of the glass is rapidly lowered so that the convective heat flux in the center decreases. The simulation results show that the window sprinkler can effectively reduce the convective heat transfer between the glass surface and the environment.

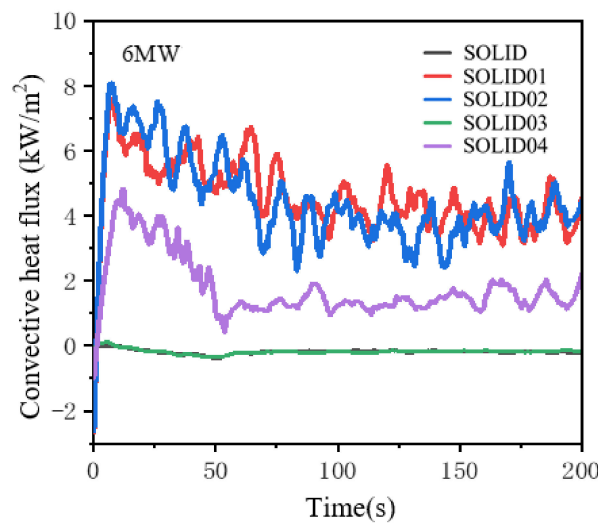


Figure 30. Convective heat flux of glass under window sprinkler conditions.

The simulated incident heat flux of the 6 MW window sprinkler is shown in Figure 31. The curves in the lower left, lower right and center are in the rising phase in the range of 0–20 s, and their maximum incident heat fluxes are 26.5 kW/m<sup>2</sup>, 27.1 kW/m<sup>2</sup> and 48.6 kW/m<sup>2</sup>, respectively. In the steady-state stage from 21 to 50 s, the steady-state incident heat fluxes were 25.1 kW/m<sup>2</sup>, 26.4 kW/m<sup>2</sup> and 46.9 kW/m<sup>2</sup>, respectively. In the range of 51–200 s, the incident heat fluxes in the lower left, lower right and center dropped to the steady-state stage, namely, 11.7 kW/m<sup>2</sup>, 12.0 kW/m<sup>2</sup> and 20.2 kW/m<sup>2</sup>, respectively. The incident heat flux in the upper left and upper right rises to about 50 kW/m<sup>2</sup>, and the incident heat flux is in a fluctuating stage. This is because with the progress of combustion, the oxygen content in the compartment continues to decrease, and the outdoor air supply affects the flame’s burning direction, such that the incident heat flux above is constantly changing in the range of 45–60 kW/m<sup>2</sup>. The simulation results show that the window sprinkler has a significant weakening effect on the incident heat flux in the lower and central areas of the glass, but has little effect on the incident heat flux above.

### 3.3. Protective Effect

The surface temperature of the glass will drop rapidly after the sprinkler is activated under the protection of the sprinkler. For the 2 MW, 4 MW and 6 MW fire sources, the window surface temperature can reach the steady-state stage. Taking the central temperature of the window as an example, the steady-state values are 40 °C, 60 °C and 76 °C, which are all controlled within the safe temperature range.

The flowing water film formed by the sprinkler on the glass surface is steady. There are three physical phenomena at play here, namely, the absorption, reflection and transmission of heat radiation by the water film, among which absorption and reflection form the blocking effect of the water film on flame radiation. The transmittance (t) of the water film to radiation can be expressed as [35]:

$$t = (1 - \alpha)^2(1 - \beta) / (1 - \alpha^2(1 - \beta)^2) \tag{5}$$

$$\alpha = (\sin^2(i_2 - i_1) / \sin^2(i_2 + i_1) + \tan^2(i_2 - i_1) / \tan^2(i_2 + i_1)) / 2 \tag{6}$$

$$\beta = 1 - e^{(-\mu L)} \tag{7}$$

$$L = d / \cos i_2 \tag{8}$$

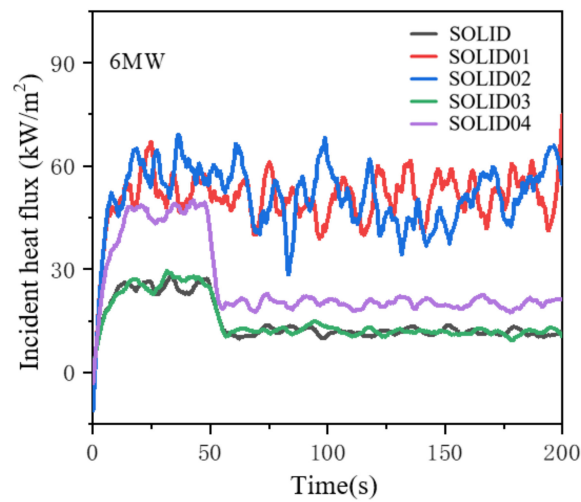


**Figure 31.** The change of the incident heat flux of the glass under the action of the window sprinkler.

In the equation,  $\alpha$  is the reflectance of the water film interface to primary radiation,  $\beta$  is the absorption ratio of the water film to primary radiation,  $i_1$  and  $i_2$  are the incident angle and the reflection angle of radiation, respectively,  $\mu$  ( $m^{-1}$ ) is the extinction coefficient of water,  $L$  (m) is the distance of radiation through the water film and  $d$  (m) is the thickness of the water film. Therefore, the transmittance of the water film to radiation can be regarded as a constant, which is only related to the thickness of the water film at this point, namely:

$$t \propto \frac{1}{d} \tag{9}$$

When the sprinkler is started, the convective heat transfer intensity on the surface of the window is extremely weak and the incident heat flux received by the window is approximately equal to the radiation of the fire source to the glass; therefore:

$$INF = t * q_r \tag{10}$$

In the equation,  $INF$  is the incident heat flux acting on the glass surface and  $q_r$  is the radiant heat flux acting on the water film at the same position on the glass surface by the fire source.

Insulation efficiency refers to the key technical parameter that characterizes the ability of fire sprinklers, with fire separation as the main function to block radiant heat. For window sprinklers, the protective effect on the window glass can be quantitatively evaluated by the heat insulation efficiency. The heat insulation efficiency of the window sprinkler can be calculated by the decay rate of the incident heat flux before and after the sprinkler has been started:

$$\mu = \left( 1 - \frac{INF_2}{INF_1} \right) * 100\% \tag{11}$$

In the equation,  $\mu$  is the heat insulation efficiency of the window sprinkler,  $INF_1$  is the incident heat flux before the sprinkler has been started and  $INF_2$  is the incident flux afterwards. Table 4 shows the heat insulation efficiency of the window sprinkler in the simulation results. The results show that the transmittance of the water film to the incident heat flux is almost independent of the HRR. The thickness of the water film at the edge is smaller than that at the center, so the transmittance is slightly larger than that at the center.

**Table 4.** Transmittance of water film to incident heat flux.

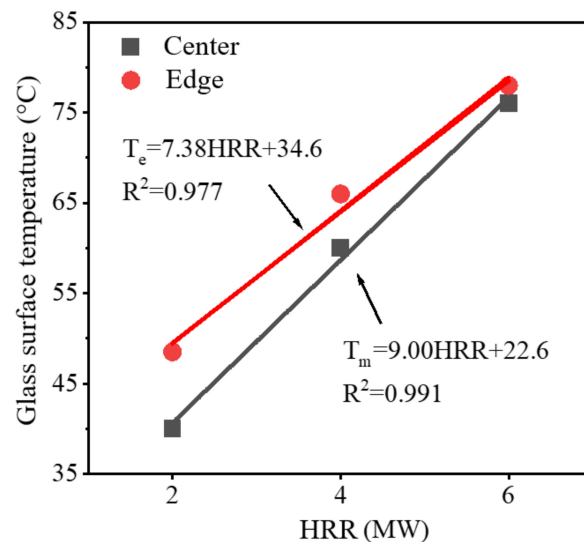
HRR (MW)	Center (%)	Edge (%)
2	58	54
4	56.5	55
6	59.4	56.5

Figure 32 shows the glass surface temperature with the heat release rate. There is a linear correlation between the glass surface temperature and HRR. The correlation fitting between HRR and the glass surface temperature can be expressed as follows:

$$T_m = 9.00HRR + 22.6 \tag{12}$$

$$T_e = 7.25HRR + 35 \tag{13}$$

where,  $T_m$  (°C) is the surface temperature at the center of the glass,  $T_e$  (°C) is the surface temperature at the edge of the glass and  $HRR$  (MW) is the heat release rate of the fire source.



**Figure 32.** Correlation between HRR and the glass surface temperature.

The window surface temperature is mainly controlled by the incident heat flux from the fire source and the heat conduction to the interior of the window. The solid heat conduction from the glass surface to its interior can be considered as one-dimensional heat conduction in a single-layer flat plate. According to Fourier’s law, the heat conduction flux of the window facing the back of the fire can be calculated by the following equation [39]:

$$q_c = -k \times \frac{T_f - T_b}{d} \tag{14}$$

where  $q_c$  (W/m<sup>2</sup>) is the heat conduction flux,  $k$  (W/(m·K)) is the heat conductivity,  $T_f$  and  $T_b$  (K) are the front and back temperatures of the window, respectively, and  $d$  is the thickness of the window.

The temperature behind the window can be obtained by Newton’s law of cooling:

$$q_d = h \times (T_b - T_e) \tag{15}$$

In the equation,  $q_d$  (W/m<sup>2</sup>) is the convective heat transfer heat flux density,  $h$  (W/(m<sup>2</sup>·K)) is the convective heat transfer coefficient and  $T_e$  (K) is the external environmental temperature.

Before the sprinkler system is started, the incident heat flux acting on the glass surface is much larger than the heat conduction from the front to the back of the window and the conduction heat flux increases with the increase of temperature difference between the two sides of the window. When sprinkler starts, the droplets form a water film on the window surface to block the heat flow and the incident heat flux decreases instantly. There is a lag in the decrease of the glass surface temperature, which leads to the incident heat flux being less than the heat conduction heat flux. When the surface temperature of the glass drops to a certain value, the heat conduction flux of the glass surface is equal to the incident heat flux received by the glass from the fire source; then, the surface temperature enters a steady state, namely:

$$q_c = -k * \frac{T_f - T_b}{d} = -INF = -t * q_r \quad (16)$$

$$T_f = \frac{t * q_r * d}{k} + T_b \quad (17)$$

Yang [40] summarized a large number of combustion test results and found that the radiant power  $q_r$  of a fire source was proportional to the power HRR of a fire source and that the proportional coefficient  $\chi$  was related to the equivalent diameter of flame, namely:

$$q_r \propto \chi HRR \quad (18)$$

$$T_f \propto \frac{t * \chi * d}{k} HRR \quad (19)$$

Therefore, the window surface temperature is proportional to the power of the fire source. The temperature at the edge is slightly higher than that at the center under the same HRR because the thickness of the water film at the edge of the window is thinner than that in the middle, which has a poor effect on the heat flow barrier.

#### 4. Conclusions

In this study, full-scale experiments on sprinkler-protected glass in building fires were carried out. The experimental process was simulated using CFD numerical simulation software (FDS) and the effect of the heat release rate on the protection effect was revealed based on the glass surface temperature and heat insulation efficiency. The main conclusions are as follows:

- (1) In a full-size compartment fire, the window sprinkler is able to protect the glass from being damaged by high-temperature smoke. Numerical simulation can effectively simulate the spray distribution pattern of a window sprinkler and the gas temperature evolution and the simulation results match well with the full-size experiments;
- (2) The window surface temperatures all decrease rapidly and increase linearly with the HRR after the window sprinkler is activated. The steady-state window center temperatures are 40 °C, 60 °C and 76 °C when the HRR is 2 MW, 4 MW and 6 MW, respectively. The window center temperature is less than the critical temperature of glass breakage, indicating that the window sprinkler can protect the glass from fire damage well, within the fire scale of 6 MW;
- (3) The thermal insulation efficiency in the edge region is slightly lesser than that in the center of the window. In the range of 2 to 6 MW, there is no significant correlation between the thermal insulation efficiency and the HRR, and the thermal insulation efficiency is in the range of 54% to 59%.

**Author Contributions:** Conceptualization, J.G., Y.J. and L.Y.; investigation, J.G. and Y.J.; writing—original draft preparation, D.W. and Y.J.; writing—review and editing, D.W. and L.Y.; project administration, J.L. and L.Y.; funding acquisition, J.L. and L.Y. All authors have read and agreed to the published version of the manuscript.

**Funding:** This work was supported by the National Science Foundation of China (No. 52076202), the Fundamental Research Funds for the Central Universities (No. WK2320000056) and the National Key R&D Program (No. 2016YFC0800604).

**Conflicts of Interest:** The authors declare that they have no known competing financial interests or personal relationships that could have appeared to influence the work reported in this paper.

## References

1. Babrauskas, V. Glass Breakage in Fires. Fire Science and Technology, Inc., 2011. Available online: [https://fireevacuationplan.ru/articles/dataFolder/to139\\_GlassBreak.pdf](https://fireevacuationplan.ru/articles/dataFolder/to139_GlassBreak.pdf) (accessed on 15 March 2022).
2. Beason, D. Fire endurance of sprinklered glass walls'. *Annu. Technol. Rev.* **1986**, *59*.
3. Emmons, H.W. The Needed Fire Science. *Fire Saf. Sci.* **1986**, *1*, 33–53. [[CrossRef](#)]
4. Dembele, S.; Rosario, R.; Wen, J.; Warren, P.; Dale, S. Simulation of Glazing Behavior in Fires using Computational Fluids Dynamics and Spectral Radiation Modeling. *Fire Saf. Sci.* **2008**, *9*, 1029–1039. [[CrossRef](#)]
5. Joshi, A.; Pagni, P. Fire-induced thermal fields in window glass. I—Theory. *Fire Saf. J.* **1994**, *22*, 25–43. [[CrossRef](#)]
6. Joshi, A.; Pagni, P. Fire-induced thermal fields in window glass. II—Experiments. *Fire Saf. J.* **1994**, *22*, 45–65. [[CrossRef](#)]
7. Gao, W.; Liu, N.; Delichatsios, M.; Yuan, X.; Bai, Y.; Chen, H.; Zhang, L. Fire spill plume from a compartment with dual symmetric openings under cross wind. *Combust. Flame* **2016**, *167*, 409–421. [[CrossRef](#)]
8. Lu, K.; Wang, Z.; Ding, Y.; Wang, J.; Zhang, J.; Delichatsios, M.A.; Hu, L. Flame behavior from an opening at different elevations on the facade wall of a fire compartment. *Proc. Combust. Inst.* **2020**, *38*, 4551–4559. [[CrossRef](#)]
9. Wang, D.; Zhou, X.; Gui, J.; Ju, X.; Ye, K.; Zhou, Z.; Cao, J.; Zheng, Y.; Cao, B.; Yang, L.; et al. Experimental study on the effect of pool fire area and violent fuel boiling on fuel burning state evolution in compartment fire. *Fuel* **2020**, *284*, 118933. [[CrossRef](#)]
10. Hassani, S.K.S.; Shields, J.; Silcock, G.W. An Experimental Investigation Into The Behaviour of Glazing in Enclosure Fire. *J. Appl. Fire Sci.* **1994**, *4*, 303–323. [[CrossRef](#)]
11. Keski-Rahkonen, O. Breaking of window glass close to fire. *Fire Mater.* **1988**, *12*, 61–69. [[CrossRef](#)]
12. Keski-Rahkonen, O. Breaking of window glass close to fire, II: Circular panes. *Fire Mater.* **1991**, *15*, 11–16. [[CrossRef](#)]
13. Kim, A.; Loughheed, G. The Protection of Glazing Systems with Dedicated Sprinklers. *J. Fire Prot. Eng.* **1990**, *2*, 49–59. [[CrossRef](#)]
14. Kim, A.K.; Taber, B.C.; Loughheed, G.D. Sprinkler Protection of Exterior Glazing. *Fire Technol.* **1998**, *34*, 116–138. [[CrossRef](#)]
15. Ng, C.M.; Chow, W.K. Review on the Design and Scientific Aspects for Drencher Systems in Different Countries. *Arch. Sci. Rev.* **2002**, *45*, 323–335. [[CrossRef](#)]
16. Wu, C.; Lin, T.; Lei, M.; Chung, T.; Huang, C.; Chiang, W. Fire Test on a Non-heat-resistant Fireproof Glass with Down-flowing Water Film. *Fire Saf. Sci.* **2005**, *8*, 327–338. [[CrossRef](#)]
17. Wu, C.W.; Lin, T.H.; Lei, M.Y.; Chung, T.H.; Huang, C.C.; Chiang, W.T. Fire resistance tests of a glass pane with down-flowing water film. *J. Chin. Inst. Eng.* **2008**, *31*, 737–744. [[CrossRef](#)]
18. Richardson, J.K.; Oleszkiewicz, I. Fire tests on window assemblies protected by automatic sprinklers. *Fire Technol.* **1987**, *23*, 115–132. [[CrossRef](#)]
19. Cai, Z.; Li, H.; Chen, L.; Cai, B.; Liao, G.; Shen, L. Experimental studies on flow field diagnosis and thermal radiation blockage of water curtain. *Fire Saf. Sci.* **2004**, *13*, 224–230.
20. Richardson, J.; Chown, G. Glazing in fire-resistant wall assemblies. *Constr. Build. Mater.* **1989**, *3*, 40–43. [[CrossRef](#)]
21. Chen, H.-T.; Lee, S.-K. Estimation of heat-transfer characteristics on the hot surface of glass pane with down-flowing water film. *Build. Environ.* **2010**, *45*, 2089–2099. [[CrossRef](#)]
22. Skelly, M.J.; Roby, R.J.; Beyler, C.L. An Experimental Investigation of Glass Breakage in Compartment Fires. *J. Fire Prot. Eng.* **1991**, *3*, 25–34. [[CrossRef](#)]
23. Voytkov, I.; Volkov, R.; Kopylov, N.; Syshkina, E.; Tomilin, A.; Strizhak, P. Impact of scattered radiation on thermal radiation shielding by water curtains. *Process Saf. Environ. Prot.* **2021**, *154*, 278–290. [[CrossRef](#)]
24. Yan, W.-M. Convective heat and mass transfer from a falling film to a laminar gas stream. *Wärme-Und Stoffübertragung* **1993**, *29*, 79–87. [[CrossRef](#)]
25. Joshi, A.A.; Pagni, P.J. *User's Guide to BREAK1, the Berkeley Algorithm for Breaking Window Glass in a Compartment Fire*; NIST: Gaithersburg, MD, USA, 1991.
26. Hietaniemi, J. *Probabilistic Simulation of Glass Fracture and Fallout in Fire*; Building and Transport; VTT: Vuorimiehentie, Finland, 2005.
27. Wang, Q.S.; Zhang, Y.; Wang, Y.; Sun, J.H.; He, L.H. Dynamic three-dimensional stress prediction of window glass under thermal loading. *Int. J. Therm. Sci.* **2012**, *59*, 152–160. [[CrossRef](#)]
28. Wang, Q.S.; Chen, H.D.; Wang, Y.; Wen, J.X.; Dembele, S.; Sun, J.H.; He, L.H. Development of a dynamic model for crack propagation in glazing system under thermal loading. *Fire Saf. J.* **2014**, *63*, 113–124. [[CrossRef](#)]
29. Pope, N.D.; Bailey, C.G. Quantitative comparison of FDS and parametric fire curves with post-flashover compartment fire test data. *Fire Saf. J.* **2006**, *41*, 99–110. [[CrossRef](#)]
30. MO, S.J.; Li, Z.R.; Liang, D.; Li, J.X.; Zhou, N.J. Analysis of smoke hazard in train compartment fire accidents base on FDS. *Procedia Eng.* **2013**, *52*, 284–289. [[CrossRef](#)]

31. Williamson, J.; Beyler, C.; Floyd, J. Validation of numerical simulations of compartment fires with forced or natural ventilation using the fire and smoke simulator (FSSIM), CFAST and FDS. In *Fire and Safety Science—Proceedings of the Tenth International Symposium, College Park, MD, USA, 19–24 June 2011*; International Association for Fire Safety Science: Gaithersburg, MD, USA, 2011; pp. 1277–1288. Available online: [https://www.researchgate.net/publication/269538155\\_Validation\\_of\\_Numerical\\_Simulations\\_of\\_Compartment\\_Fires\\_with\\_Forced\\_or\\_Natural\\_Ventilation\\_Using\\_the\\_Fire\\_and\\_Smoke\\_Simulator\\_FSSIM\\_CFAST\\_and\\_FDS](https://www.researchgate.net/publication/269538155_Validation_of_Numerical_Simulations_of_Compartment_Fires_with_Forced_or_Natural_Ventilation_Using_the_Fire_and_Smoke_Simulator_FSSIM_CFAST_and_FDS) (accessed on 10 March 2022).
32. McGrattan, K.; Hostikka, S.; McDermott, R.; Floyd, J.; Weinschenk, C.; Overholt, K. Fire dynamics simulator user’s guide. *NIST Spec. Publ.* **2013**, *1019*, 1–339.
33. Forney, G.P. Smokeview (Version 5)—A Tool for Visualizing Fire Dynamics Simulation Data, Volume I: User’s Guide. 2017. Available online: <https://www.govinfo.gov/content/pkg/GOVPUB-C13-aacc825870ad71263dbcdeba3c138adf/pdf/GOVPUB-C13-aacc825870ad71263dbcdeba3c138adf.pdf> (accessed on 20 March 2022).
34. Quintiere, J.G.; Wade, C.A. Compartment Fire Modeling. In *SFPE Handbook of Fire Protection Engineering*; Springer: New York, NY, USA, 2016; pp. 981–995.
35. Wang, Y.; Wang, Q.; Sun, J.; He, L.; Liew, K.M. Thermal performance of exposed framing glass façades in fire. *Mater. Struct.* **2016**, *49*, 2961–2970. [[CrossRef](#)]
36. Gui, J.; Yang, Q.; Zhu, L. A method to evaluate fire water supply partitions in super high-rise buildings. In *IOP Conference Series: Earth and Environmental Science*; IOP Publishing: Bristol, UK, 2019; Volume 227, p. 042018.
37. Gui, J.; Wang, D.; Jiang, Y.Q.; Zheng, Y.; Ye, K.; Huang, D.Y.; Yang, L.Z. Full-scale Experimental study on the suppression effect of water sprinkler system on energy saving building fire. In *IOP Conference Series: Earth and Environmental Science*; IOP Publishing: Bristol, UK, 2019; Volume 354, p. 012096.
38. Possidente, L.; Weiss, A.; de Silva, D.; Pustorino, S.; Nigro, E.; Tondini, N. Fire safety engineering principles applied to a multi-storey steel building. *Proc. Inst. Civ. Eng.-Struct. Build.* **2021**, *174*, 725–738. [[CrossRef](#)]
39. Nigro, E.; Bilotta, A.; Asprone, D.; Jalayer, F.; Prota, A.; Manfredi, G. Probabilistic approach for failure assessment of steel structures in fire by means of plastic limit analysis. *Fire Saf. J.* **2014**, *68*, 16–29. [[CrossRef](#)]
40. Yang, J.C.; Hamins, A.; Kashiwagi, T. Estimate of the Effect of Scale on Radiative Heat Loss Fraction and Combustion Efficiency. *Combust. Sci. Technol.* **1994**, *96*, 183–188. [[CrossRef](#)]